



# Three donor-acceptor polymeric electrochromic materials employing 2,3-bis(4-(decyloxy)phenyl)pyrido[4,3-b]pyrazine as acceptor unit and thiophene derivatives as donor units



Hui Zhao<sup>a</sup>, Yuanyuan Wei<sup>a,b</sup>, Jinsheng Zhao<sup>b,\*</sup>, Min Wang<sup>b,\*</sup>

<sup>a</sup> College of Chemical Engineering, China University of Petroleum (East China), QingDao 266580, PR China

<sup>b</sup> Shandong Key laboratory of Chemical Energy Storage and Novel Cell Technology, Liaocheng University, Liaocheng 252059, PR China

## ARTICLE INFO

### Article history:

Received 25 July 2014

Received in revised form 7 September 2014

Accepted 9 September 2014

Available online 16 September 2014

### Keywords:

Donor-acceptor polymers

Thiophene derivatives

pyrido[3,4-b] pyrazine

Electrochromism

## ABSTRACT

In this study, 5,8-dibromo-2,3-bis(4-(decyloxy) phenyl) pyrido[4,3-b]pyrazine was synthesized and used as the acceptor unit, which then be coupled with three thiophene derivatives (3-methylthiophen, 3-methoxythiophen and 3,4-dimethoxythiophen) to give rise to three novel monomers, 2,3-bis(3-methoxythiophen and 3,4-dimethoxythiophen) to give rise to three novel monomers, 2,3-bis(4-(decyloxy) phenyl)-5,8-bis(3-methylthiophen-2-yl) pyrido[4,3-b]pyrazine (**M1**), 2,3-bis(4-(decyloxy) phenyl)-5,8-bis(3-methoxythiophen-2-yl) pyrido[4,3-b]pyrazine (**M2**) and 2,3-bis(4-(decyloxy) phenyl)-5,8-bis(3,4-dimethoxythiophen-2-yl) pyrido [4,3-b]pyrazine (**M3**). The corresponding polymers **P1**, **P2**, **P3** were obtained by electropolymerization method. These polymers were characterized in terms of their spectroelectrochemical and electrochemical properties by cyclic voltammetry and UV-Vis-NIR spectroscopy. The band gaps of the polymers were calculated based on the spectroelectrochemistry analysis, and were 1.39 eV, 1.136 eV and 1.25 eV for **P1**, **P2**, **P3**, respectively. Electrochromic investigations showed that **P1** switched between blue and colorless transmissive state, **P2** switched between green to transmissive light gray color, and **P3** switched between blue to transmissive light brown color. Electrochromic switching studies showed that all three polymers exhibit high coloration efficiency, fast response time, and express more than 45% change in the transmittance in the near-IR region, which could make these polymers useful in applications in NIR electrochromic devices.

© 2014 Elsevier Ltd. All rights reserved.

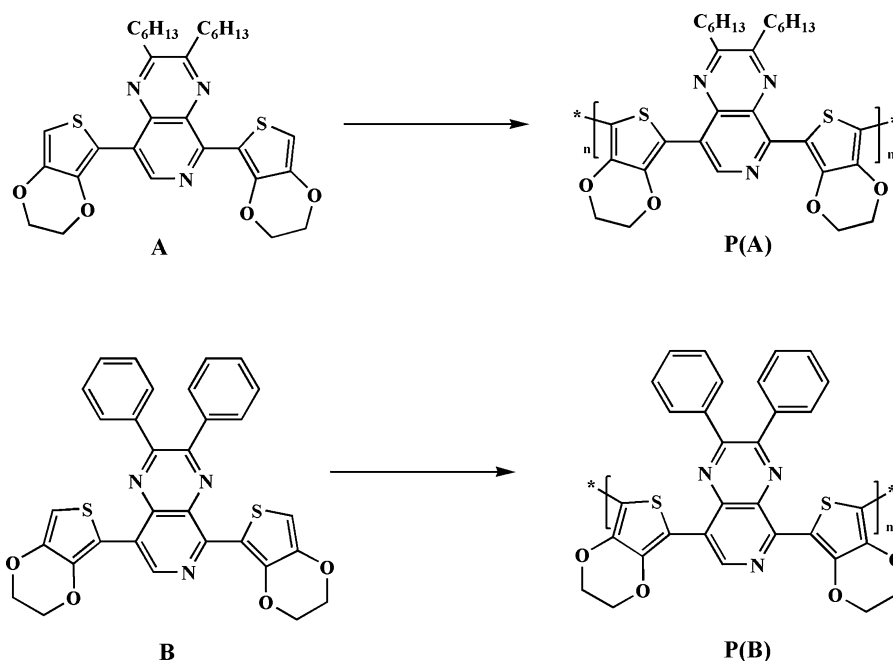
## 1. Introduction

Considering the unique properties such as attainability of faster response times, higher contrast ratios, color tenability via structural modification and easy processibility (e.g. electrochemical deposition, spin coating and spray coating), conjugated polymers (CPs) are bound to be promising materials of today's world and are extensively applied in the fields of displays[1], energy-saving “smart” windows[2], field-effect transistors[3], sensors[4] and memory devices[5]. Recently, low band gap conjugated polymers have received considerable interest, specifically those with band gaps below 1.5 eV [6]. One efficient way to design low band gap polymers is to alternate electron donor (D) and acceptor (A) units in the conjugated backbone of the polymers, i.e. D-A approach. The major advantage of the D-A approach is that

proper choice of the donor and acceptor groups allows one to select the approximate HOMO and LUMO energies of the resulting polymer. These low band gap polymers are typically colored in their neutral state as their  $\pi-\pi^*$  transition lies in the visible or even the near-infrared region of the electromagnetic spectrum. The materials become more transparent to the eye upon doping, as the  $\pi-\pi^*$  transition is bleached and lower-energy electronic transitions, which absorb in the IR, is developed [7]. Therefore, many different types of low band gap polymers have been synthesized and developed for this purpose. 1,2,3-benzothiadiazole[8], thieno[3,4-b]pyrazine[9], 2,1,3-benzothiadiazole[10], quinoxaline[11,12], are mostly preferred acceptor type units to design donor-acceptor type low band gap molecules. Quinoxaline derivatives (Qx) have been demonstrated to be an admirable building block for synthesis of low band gap conjugated polymers due to their electron withdrawing feature of two imine nitrogens in the Qx. In terms of providing the utility of introducing substituents easily on the 2 and 3 positions of itself, the Qx unit has a great structure for controlling the electronic structure of the ending polymers [13].

\* Corresponding authors.

E-mail addresses: [j.s.zhao@163.com](mailto:j.s.zhao@163.com) (J. Zhao), [wangmin1724@163.com](mailto:wangmin1724@163.com) (M. Wang).



**Scheme 1.** The previously reported polymers employing pyrido[3,4-*b*] pyrazines as the acceptor unit for optoelectronic applications.

Pyrido[3,4-*b*] pyrazine is a kind of compounds with the similar molecular structure of Qx, which exhibits a more stronger electron-withdrawing effect than that of Qx due to the presence of the additional pyridine N-atoms. On the basis of the synthesis of the monomers depicted in Scheme 1, polymer (A) and Polymer (B) have been electrochemically synthesized and characterized in terms of their electrochromic properties [7,14]. Both polymers showed a valuable neutral green color in addition to their stable oxidation and reduction (p- and n-type doping) processes, and the detailed characterizations varied with the substituents in the 2 and 3 positions of pyrido[3,4-*b*] pyrazine ring. It has clearly been demonstrated that alkyl side chains not only enhance the ease of processing, but also modify the electronic properties of the conjugated polymers [15]. The oxidation potential of the polymers, stability of the oxidized state, and band gap can drastically be altered upon insertion of strong electron-donating alkoxy side chains in the polymer backbone [16].

On the other hand, 3,4-ethylenedioxythiophene (EDOT), EDOT derivatives and thiophene are most frequently used as the donor units for the construction of D-A-D type monomers. In one of our recent work, the use of 3-methoxythiophene as the donor unit also led to the formation of low band gap polymers, with low oxidation potential, ease of electrochemical polymerization and robust stabilities [17]. Besides 3-methoxythiophene, 3-methylthiophene and 3,4-dimethoxythiophene are never used as the donor units with a pyrido[3,4-*b*] pyrazine acceptor unit in D-A type polymers.

Based on the above considerations, in this study, we synthesized three novel monomers including 2,3-bis(4-decyloxy) phenyl)-5,8-bis(3-methylthiophen-2-yl) pyrido[4,3-*b*]pyrazine (**M1**), 2,3-bis(4-decyloxy) phenyl)-5,8-bis(3-methoxythiophen-2-yl) pyrido[4,3-*b*]pyrazine (**M2**) and 2,3-bis(4-decyloxy) phenyl)-5,8-bis(3,4-dimethoxythiophen-2-yl) pyrido[4,3-*b*]pyrazine (**M3**), using 2,3-bis(4-(decyloxy) phenyl) pyrido[4,3-*b*]pyrazine as the acceptor unit. The introduction of 4-(decyloxy) phenyl substituent on the 2 and 3 positions of the pyrido[4,3-*b*]pyrazine ring enhanced the solubility of the monomers, which is beneficial to the handling of the electropolymerization processing in conventional solvent. Through electrochemical deposition method their

corresponding polymers including **P1**, **P2**, and **P3** were obtained. Then the electrochemical and electrochromic properties of these polymers were characterized by using cyclic voltammetry (CV), UV-Vis-NIR spectroscopy, fluorescence spectra and scanning electron microscopy (SEM). **P1** exhibited a color change from light blue to a colorless transmissive, while **P3** switched between blue to a transmissive brown state. It is particularly worth mentioning here is that the polymer film of **P2** showed a green color in the neutral state and turned to transmissive gray upon oxidation. From the results, the thiophene derivatives with electron-donating groups can successfully tailor the electrochromic properties by combining a low monomer oxidation potential and a narrow band gap as well as the high electrical conductivity. Out of our expectation, although the electron-donating ability of tributyl(3,4-dimethoxythiophen-2-yl) stannane is stronger than that of tributyl(3-methoxythiophen-2-yl) stannane, **P3** experienced a blue shift when compared to **P2**, which may be attributed to the steric hindrance effect.

## 2. Experimental section

### 2.1. General

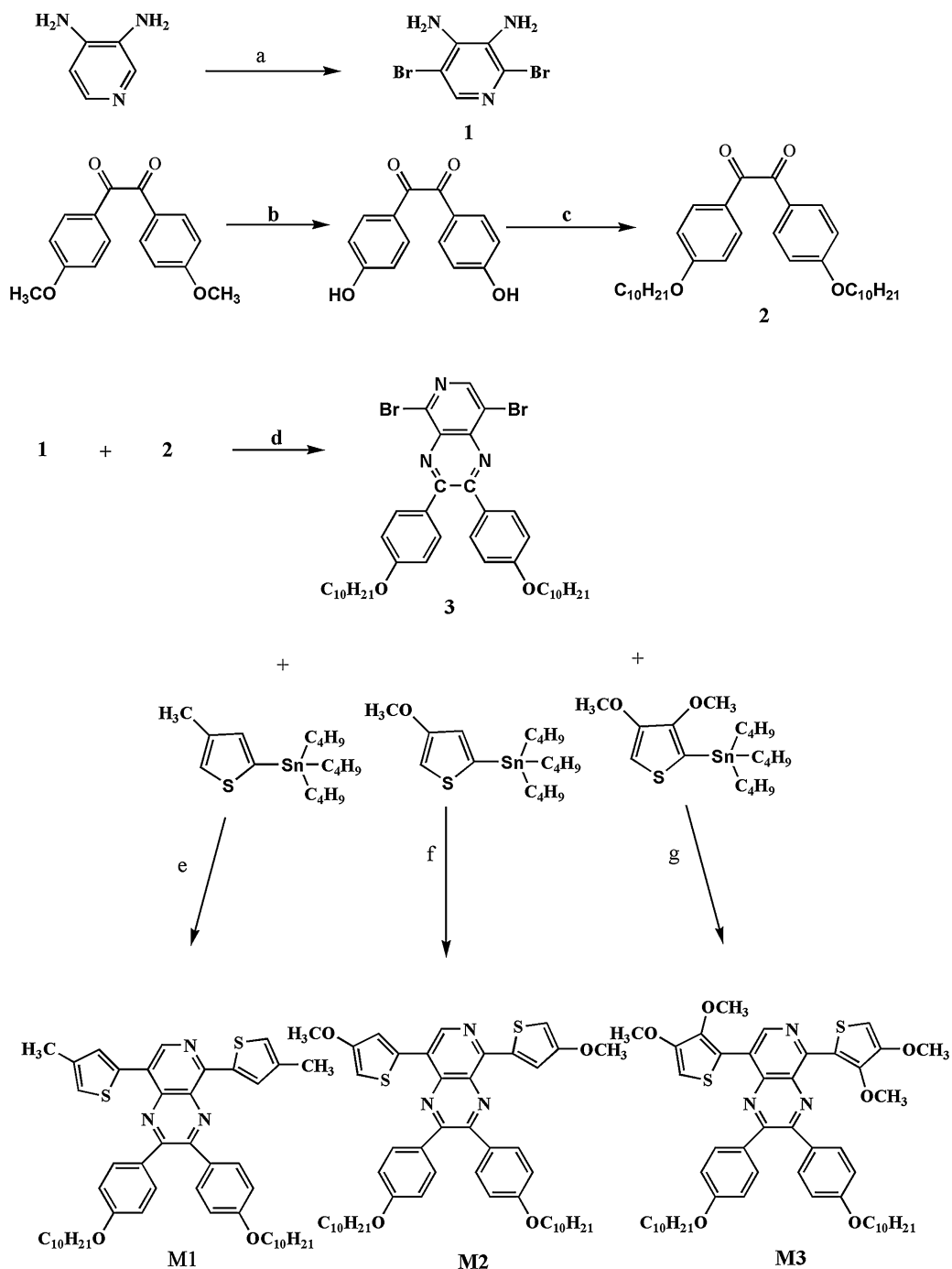
All chemicals except indicated otherwise were purchased from Aldrich Chemical as analytical grade without further purification methods. 3,4-diamino-2,5-dibromopyridine and 1,2-bis(4-(decyloxy) phenyl) ethane-1,2-dione were synthesized according to the previously reported literature methods. <sup>1</sup>H NMR and <sup>13</sup>C NMR spectroscopy studies were performed on a Varian AMX 400 spectrometer, which use tetramethylsilane (TMS) as the internal standard. Electrochemical synthesis and experiments were carried out in a one-compartment cell with a CHI760 Electrochemical Analyzer controlled by a computer, employing a platinum wire with a diameter of 0.5 mm as a working electrode, a platinum ring as a counter electrode, and a silver wire (Ag wire) as a pseudo-reference electrode. Scanning electron microscope (SEM) measurements were taken by using a Hitachi SU-70 thermionic field emission SEM. The thicknesses of the polymers were tested by Step

Profiler. In situ spectroelectrochemistry was performed using a Varian Cary 5000 UV-Vis-NIR spectrophotometer with a measurement range that extended from 200 nm in the UV to 3300 nm in the NIR. The polymer films were potentiostatically deposited onto transparent electrodes of ITO/glass (the active area:  $0.9\text{ cm} \times 3.0\text{ cm}$ ) which placed in a quartz cuvette that allowed for placement of the transparent electrode, Pt wire counter electrode, and Ag wire pseudo reference. Digital photographs of the polymer films were taken by a Canon Power Shot A3000 IS digital camera. Fluorescence spectra were performed on a F-380 Fluorospectro Photometer instrument combined with a computer.

## 2.2. Synthesis

### 2.1. 3,4-diamino-2,5-dibromopyridine (1)

The synthesis of 3,4-diamino-2,5-dibromopyridine was improved on the basis of the method reported in a literature [18]. The mixture of pyrido-3,4-diamine (2 g, 18.3 mmol) with an aqueous HBr (48%, 30 ml) were prepared in a 250 ml three-neck round-bottom flask with a magneton inside. After the mixture was heated to  $100\text{ }^\circ\text{C}$ , bromine (2.5 ml) was added dropwise, and the solution was stirred for 5 h at  $135\text{ }^\circ\text{C}$ . After the mixture was cooled to room temperature, an aqueous solution of  $\text{Na}_2\text{S}_2\text{O}_3$ , an aqueous solution



**Scheme 2.** Synthetic route of the monomers. (a) HBr,  $\text{Br}_2$ ,  $135\text{ }^\circ\text{C}$ , 5 h. (b) HAc, HBr, reflux, 12 h. (c) DMF,  $\text{K}_2\text{CO}_3$ , 1 - bromine decane, TBAB,  $120\text{ }^\circ\text{C}$ , 90 min. (d)  $50\text{ }^\circ\text{C}$ , 12 h. (e-g)  $\text{Pd}(\text{PPh}_3)_2\text{Cl}_2$ , tributyl(3-methylthiophen-2-yl) stannane (e), tributyl(3-methoxythiophen-2-yl) stannane (f), tributyl(3,4-dimethoxythiophen-2-yl) stannane (g), dry toluene, reflux, 24 h.

of  $\text{Na}_2\text{CO}_3$ , and distilled water were added in this order to get a yellow precipitate. Then the precipitate was separated by filtration and washed with distilled water three times. Recrystallization from the mixture solution of toluene: THF (v:v=5:1) gave white flocculence solid, yielded: 50%.  $^1\text{H}$  NMR (DMSO, 400 MHz, ppm):  $\delta$ = 7.53 (s, 1H), 5.99 (s, 2H), 5.03 (s, 2H).  $^{13}\text{C}$  NMR (DMSO, 101 MHz, ppm):  $\delta$ = 139.93, 139.13, 129.54, 126.67, 106.22 (see Fig. S1 in Supporting Informations).

## 2.2. 1,2-bis(4-(decyloxy) phenyl) ethane-1,2-dione (2)

The synthesis of **2** needs two steps. Firstly, a mixture of 1,2-bis(4-methoxyphenyl) ethane-1,2-dione (3 g, 11 mmol), glacial acetic acid (30 ml) and HBr (48%, 100 ml) were added into a three-neck round bottom flask orderly, heated to reflux and stirred for 12 h. Then the mixture was cooled to room temperature and brown precipitation was observed. Then the precipitate was separated by filtration and washed with distilled water three times to give 1,2-bis(4-hydroxyphenyl) ethane-1,2-dione, yield: 75%. Secondly, 1,2-bis(4-hydroxyphenyl) ethane-1,2-dione (2.0 g, 8.2 mmol), 1-bromodecane (4.04 g, 3.78 mmol), anhydrous potassium carbonate (2.4 g, 0.24 mol) and Tetra-n-butylammonium bromide (1.33 g, 4.13 mmol) were dissolved in DMF (120 ml). The solution was heated to 120 °C and reacted for 90 min. After reaction, the solution was cooled to room temperature, added with water, oscillated by ultrasonic instrument. The cream-color deposit was filtered and washed by distilled water several times to give the target product (**2**) with a high productivity (about 90%).  $^1\text{H}$  NMR ( $\text{CDCl}_3$ , 400 MHz, ppm):  $\delta$ = 7.92 (m, 4H, ArH), 6.94 (m, 4H, ArH), 4.02 (t, 4H), 1.80 (m,

4H), 1.45 (m, 4H), 1.33 (m, 24H), 0.88 (t, 6H).  $^{13}\text{C}$  NMR ( $\text{CDCl}_3$ , 101 MHz, ppm):  $\delta$ = 189.03, 159.95, 127.81, 121.54, 110.17, 63.94, 27.35, 25.61, 25.00, 24.75, 21.40, 18.14 (see Fig. S2 in Supporting Informations).

## 2.3. 5,8-dibromo-2,3-bis(4-(decyloxy) phenyl) pyrido[4,3-b]pyrazine (3)

A solution of 2,5-diromopyridine-3,4-diamine (1 g, 3.74 mmol) and 1,2-bis(4-(decyloxy) phenyl) ethane-1,2-dione (1.955 g, 3.74 mmol) which dissolved in glacial acetic acid (60 ml) was heated to 50 °C and stirred for 12 h under argon atmosphere. At the end of the reaction, yellow sediment was observed. Then the solution was cooled to room temperature and filtered. The separated solid was washed with distilled water several times and dried under vacuum oven to give a yellow flocculent precipitate, yielded: 90%.  $^1\text{H}$  NMR ( $\text{CDCl}_3$ , 400 MHz, ppm):  $\delta$ = 8.68 (s, 1H), 7.67 (m, 4H, ArH), 6.88 (m, 4H, ArH), 4.00 (t, 4H), 1.80 (m, 4H), 1.42 (m, 28H), 0.88 (t, 6H).  $^{13}\text{C}$  NMR ( $\text{CDCl}_3$ , 101 MHz, ppm):  $\delta$ = 161.50, 161.18, 157.85, 156.77, 146.85, 146.00, 136.82, 132.14, 131.87, 129.80, 120.16, 114.75, 68.43, 32.11, 29.57, 26.24, 22.89, 14.32 (see Fig. S3 in Supporting Informations).

## 2.4. Synthesis of M1, M2 and M3

5,8-dibromo-2,3-bis(4-(decyloxy) phenyl) pyrido[4,3-b]pyrazine (2 g, 2.65 mmol) and tributyl(3-methylthiophen-2-yl) stannane (5.3 mmol) or tributyl(3-methoxythiophen-2-yl) stannane (5.3 mmol) or tributyl(3,4-dimethoxythiophen-2-yl) stannane (5.3 mmol) were dissolved in anhydrous toluene (80 ml) and Pd( $\text{PPh}_3$ ) $_2\text{Cl}_2$  (0.2 g, 2.85 mmol) was added at room temperature.

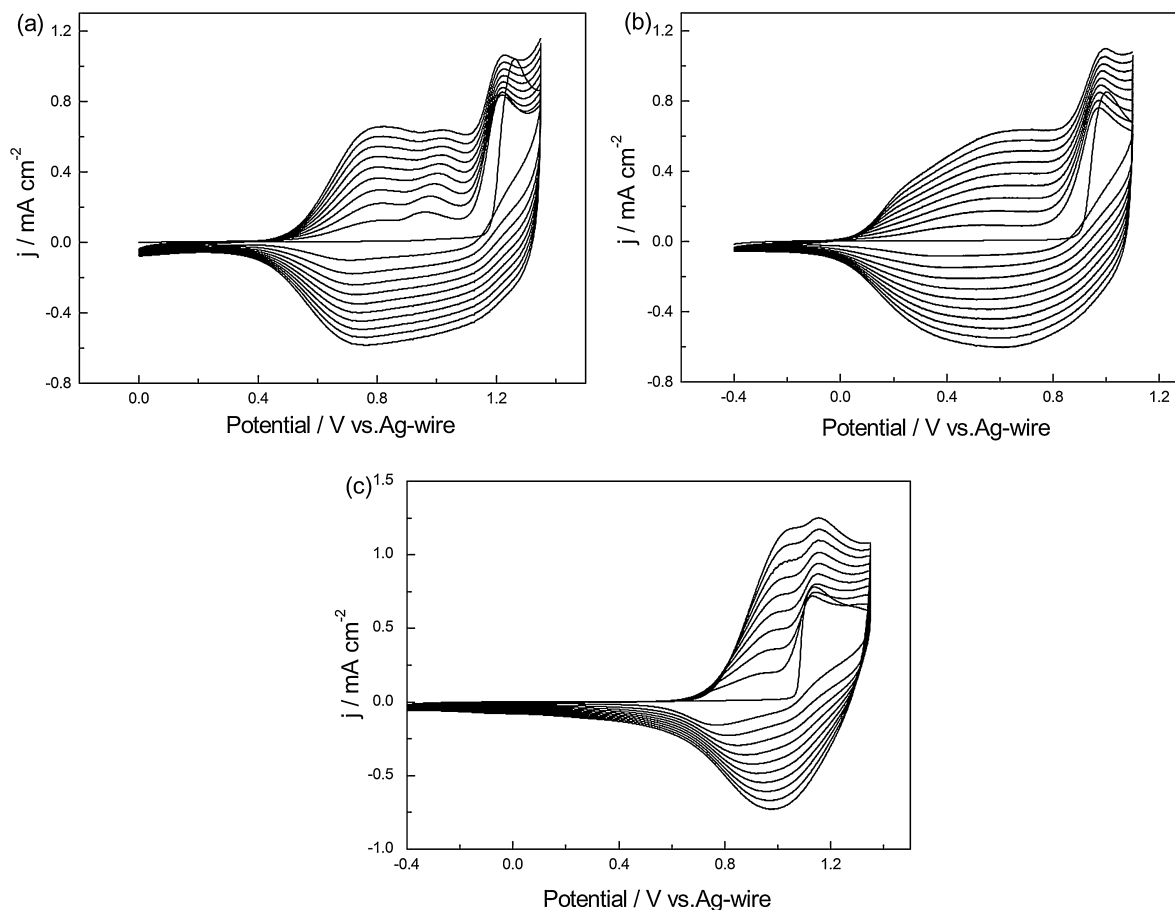


**Fig. 1.** Cyclic voltammogram curves of **M1** (a), **M2** (b) and **M3** (c) in 0.2 M TBAPF $_6$ /DCM/ACN solution at a scan rate of 100 mV s $^{-1}$  respectively.  $j$  denotes the current density.  $E$  denotes the potential.

Raise the temperature gradually until the solution was refluxed (about 123 °C). The mixture was stirred under argon atmosphere for 24h, cooled and concentrated by evaporating toluene under reduced pressure. The residue was purified by column chromatography on silica gel using hexane-dichloromethane as the eluent. The purified product M1 is bright red solid.  $^1\text{H}$  NMR ( $\text{CDCl}_3$ , 400 MHz, ppm):  $\delta$ =9.04 (s, 1H), 8.39 (s, 1H), 7.77 (m, 4H, ArH), 7.66 (m, 1H), 7.11 (s, 1H), 7.15 (s, 1H), 6.91 (m, 4H, ArH), 4.01 (m, 4H), 1.81 (m, 4H), 1.39 (m, 12H), 1.29 (m, 12H), 0.91 (t, 6H).  $^{13}\text{C}$  NMR ( $\text{CDCl}_3$ , 101 MHz, ppm):  $\delta$ =160.85, 160.54, 155.32, 152.95, 151.04, 143.39, 140.76, 139.83, 138.37, 137.62, 136.25, 133.24, 132.28, 131.88, 131.02, 130.68, 128.78, 126.83, 124.86, 124.45, 114.55, 68.35, 32.12, 29.62, 26.28, 22.91, 14.34 (see Fig. S4 in Supporting Informations). The purified product M2 is dark red solid.  $^1\text{H}$  NMR ( $\text{CDCl}_3$ , 400 MHz, ppm):  $\delta$ = 9.00 (s,1H), 8.30 (d, 1H), 7.70 (m, 4H, ArH), 6.90 (m, 4H, ArH), 6.52 (d, 1H), 6.46 (d, 1H), 4.00 (m, 4H), 3.97 (d, 6H), 1.80 (m, 4H), 1.35 (m, 28H), 0.90 (t, 6H).  $^{13}\text{C}$  NMR ( $\text{CDCl}_3$ , 101 MHz, ppm):  $\delta$ = 160.90, 160.58, 159.00, 158.65, 155.53, 153.25, 150.56, 143.18, 139.95, 136.35, 132.50, 132.24, 131.82, 130.93, 130.55, 124.22, 122.58, 118.39, 114.60, 103.28, 100.99, 68.35, 57.53, 32.12, 29.58, 26.28, 22.90, 14.34(see Fig. S5 in Supporting Informations). The purified product M3 is also dark red solid.  $^1\text{H}$  NMR ( $\text{CDCl}_3$ , 400 MHz, ppm):  $\delta$ = 9.6 (s, 1H), 7.7 (m, 4H, ArH), 6.87 (m, 4H, ArH), 6.49 (s, 1H), 6.45 (s, 1H), 3.91 (s, 6H), 3.85 (s, 6H), 3.77 (m, 4H), 1.79 (m, 4H), 1.33 (m, 28H), 0.89 (t, 6H).  $^{13}\text{C}$  NMR ( $\text{CDCl}_3$ , 101 MHz, ppm):  $\delta$ = 160.83, 160.50, 155.09, 152.60, 151.16, 150.96,

145.60, 139.96, 133.04, 132.28, 131.94, 130.96, 130.67, 123.41, 118.44, 114.55, 100.93, 99.88, 68.34, 61.17, 60.54, 57.48, 57.61, 32.09, 29.57, 26.25, 22.86, 14.27 (see Fig. S6 in Supporting Informations).

### 3. Results and discussion

#### 3.1. Synthesis of monomers

The synthetic route to the monomers is shown in Scheme 2. First, 3,4-diamino pyridine was brominated at the 2 and 5 positions with bromine in 48% HBr to yield 3,4-diamino-2,5-dibromopyridine(1) [18]. Second, 1,2-bis(4-methoxyphenyl) ethane-1,2-dione was hydroxylated in the mixed solution of HAC/HBr and then alkylated in the presence of DMF, 1 - bromine decane, anhydrous potassium carbonate and Tetra-n-butylammonium bromide (TBAB) to produce 1,2-bis(4-(decyloxy) phenyl) ethane-1,2-dione (2). **1** and **2** were mixed in ice acetic acid solution to produce a yellow flocculent precipitate (**3**) by a condensation reaction. Finally, the condensation product was reacted with corresponding tributylstannane in the presence of a catalytic amount of Pd ( $\text{PPh}_3$ ) $_2\text{Cl}_2$  to generate the end product **M1**, **M2** and **M3** with satisfactory yields, respectively.

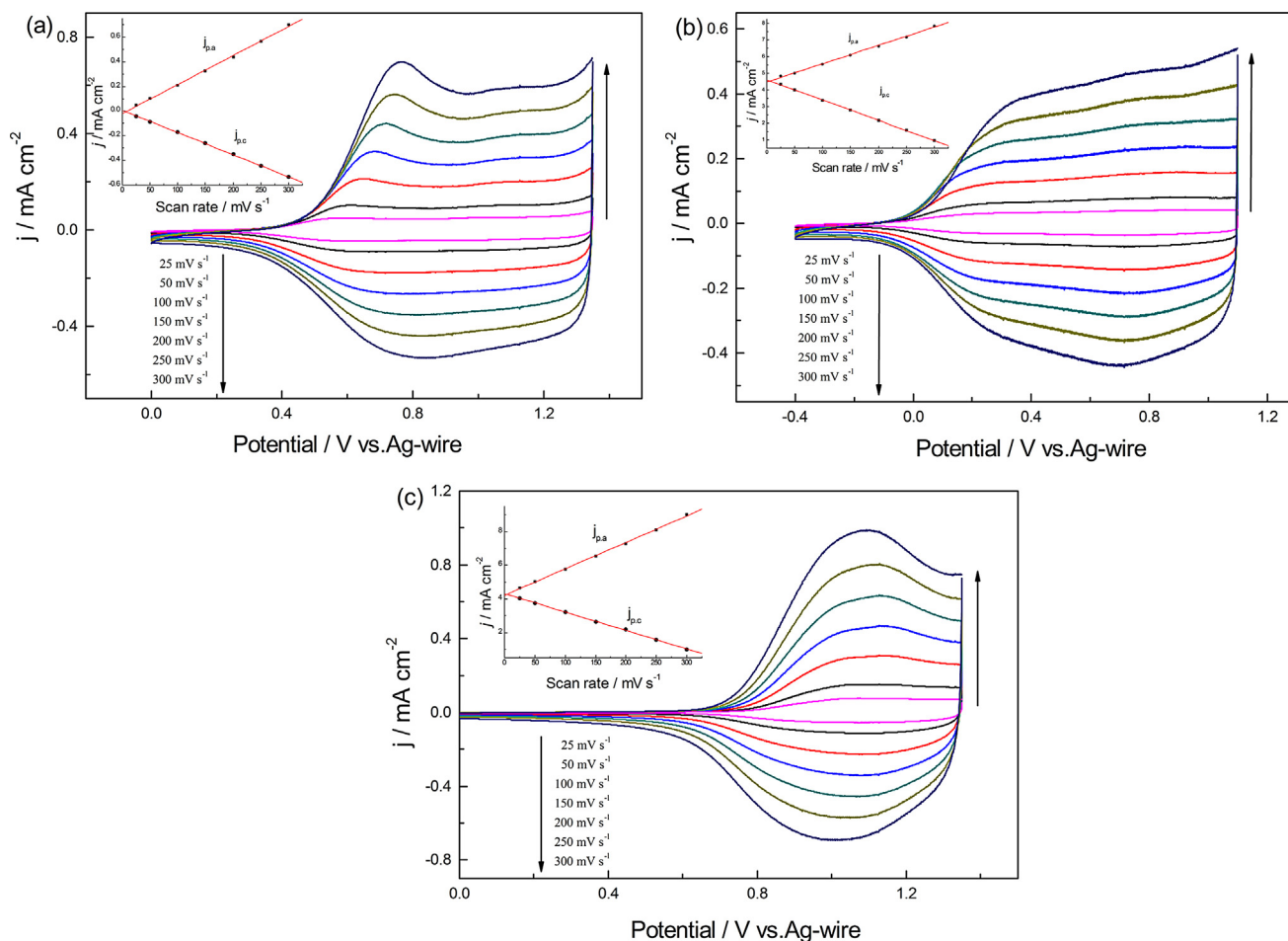


Fig. 2. CV curves of the P1 (a), P2 (b) and P3 (c) film at different scan rates between 25 and 300  $\text{mV s}^{-1}$  in the monomer-free 0.2 M TBAPF $_6$ /ACN/DCM solution, respectively.

### 3.2. Electrochemical polymerization and characterization

All of the three polymers were polymerized on the platinum wire (the diameter is 0.5 mm) by cyclic voltammogram (CV) with the same potential scan rate ( $100 \text{ mV s}^{-1}$ ) to characterize both the monomer oxidation potential and the polymer electrochemistry during film deposition. Fig. 1 displayed the continuous CV curves of the monomers including **M1**, **M2** and **M3** in given concentration in ACN/DCM (1:1, by volume) solution containing 0.2 M tetrabutylammonium hexafluorophosphate (TBAPF<sub>6</sub>) as a supporting electrolyte. The first cycle of the curve is attributed to the oxidation of the monomer. Irreversible monomer oxidation peak was appeared at 1.26 V for **M1**, 1.0 V for **M2** and 1.1 V for **M3** and the onset oxidation potentials ( $E_{\text{onset}}$ ) of **M1**, **M2** and **M3** were calculated as 1.17 V, 0.91 V and 1.1 V, respectively. Concomitant increase in the current intensities indicated the characteristic behavior of the formation of a deposited electroactive film on the working electrode surface. As shown in Fig. 1, the voltammograms suggested that all three monomers showed more than one oxidation process and a broad reduction process. The CV curves of M1 showed a cathodic peak at around 0.75 V and the corresponding two shoulder-like oxidation peaks were found at about 0.81 V (Fig. 1a). Similarly, the CV curves of M2 exhibited a reduction peak at about 0.63 V and two oxidation peaks at about 0.67 V and 0.90 V respectively (Fig. 1b), the CV curves of M3 displayed a reduction peak at about 1.0 V and an obvious oxidation peak at about 1.15 V (Fig. 1c). Compared to **M1**, the redox potentials were decreased for **M2/M3**, which mainly due to the ability to contribute electrons of 3-methoxy/3,4-dimethoxy group on thiophene ring is much stronger than that of 3-methyl group. However, out of our expectation, the onset oxidation potential ( $E_{\text{onset}}$ ) of **M3** is slightly more positive than that of **M2**. This may be because of the steric-hindrance effect. As can be seen from the structure of **M3**, since two methoxyl groups are located on the adjacent location of thiophene ring, the steric-hindrance effect is greatly strengthened. This is likely to make a dent in their conjugative effect, which leads to a higher  $E_{\text{onset}}$ .

For the sake of detecting the properties of the polymer films, the polymer-coated electrode was removed from the monomer solution and rinsed with DCM/ACN before being immersed in an electrolyte solution containing 0.2 M TBAPF<sub>6</sub> in DCM/ACN. The polymer films were then cycled between their redox potentials ranges at different scan rates from 300 to  $25 \text{ mV s}^{-1}$  (Fig. 2). A linear increase in the peak currents as a function of the scan rates confirmed well-adhered electroactive polymer films on the

electrode surface as well as non-diffusional redox process [19], as shown in the figure insert. A redox process of p-doping was observed between 0.45 V and 1.2 V for **P1**, between 0.04 V and 1.0 V for **P2** and between 0.65 V and 1.3 V for **P3**. In addition, to investigate the stability characteristic, the three polymer films were deposited on a Pt electrode using CV method in TBAPF<sub>6</sub>/DCM/ACN as described above. Then the polymer films were cycled between doped and neutral states for 1000 times with a scan rate of  $200 \text{ mV s}^{-1}$  in 0.1 M lithium perchlorate/propylene carbonate (PC) electrolyte/solvent couple (as shown in Fig. 3). From the figure, after 1000 cycles, **P2** still remained a high stability without any considerable charge loss (about 1.4%). Although the stabilities of **P1** and **P3** are not as steady as that of **P2**, they also had an acceptable stability since **P1** retained 87.2% of its electroactivity and **P3** retained 76.8% of its electroactivity both after regular 1000 cycles (see Fig. S7 in Supporting Informations). Then a conclusion can be arrived at that all three polymer films have a long-term switching stability between redox states, especially in the case of **P2**, which makes them to meet the severe requirement for electrochromic polymers, thus to be outstanding candidates for commercial device applications.

As described previously, polymers of this system usually not only have low band gap but also can reveal n-doped character. However, systems that exhibit n-type doping are less commonly obtained due to practically inaccessible reduction potentials and instability of organic anions, especially to water and oxygen [13]. Fig. 4 displayed the both n-doping and p-doping process of the three polymers at a scan rate of  $100 \text{ mV s}^{-1}$ . The potentials were swept between -0.4 and 1.1 V for p-doped spectra, -0.40 and -1.8 V for n-doped spectra for **P2**. Scanning intervals were 0.0 and 1.35 V for p-doped spectra and 0.0 and -1.8 V for n-doped spectra for both **P1** and **P3**. As is shown in the picture, **P2** has revealed perfect n-doping process, and displayed an  $E_{1/2}$  of -1.18 V. In addition, the redox peak of the n-doping/dedoping is much stronger than the p-doping/dedoping process. This behavior has been noted previously in similar systems and is attributed to both n-doping and a redox transport mechanism with the lack of a capacitive character indicative of a localized anionic state rather than the delocalized state required for significant n-type conductivity [14,20]. Nevertheless, the n-doping processes of **P1** and **P3** were too weak to be observed. This is most likely due to the decomposition of the polymers at the high negative potentials, which may catalyzed by the presence of oxygen and traceful amount of waters in the solvents, since the measurements were conducted in the ambient temperature environment.

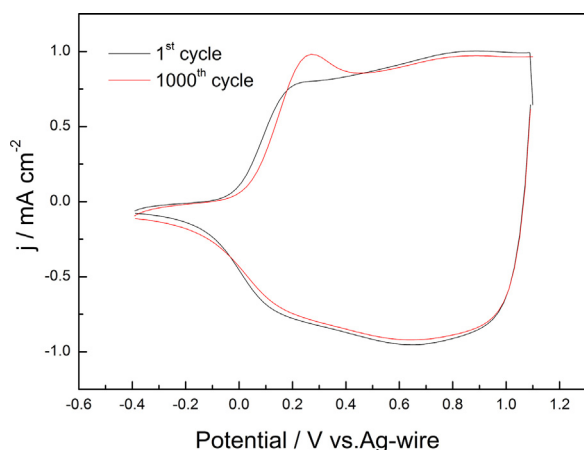


Fig. 3. The first and the 1000th CV curve of the **P2** film at a scan rate of  $200 \text{ mV s}^{-1}$  in 0.1 M lithium perchlorate/propylene carbonate (PC) electrolyte/solvent couple.

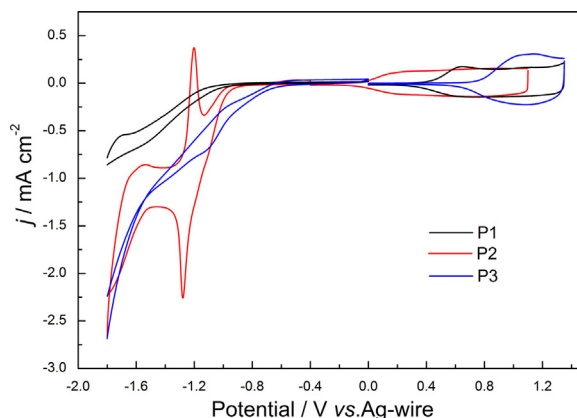
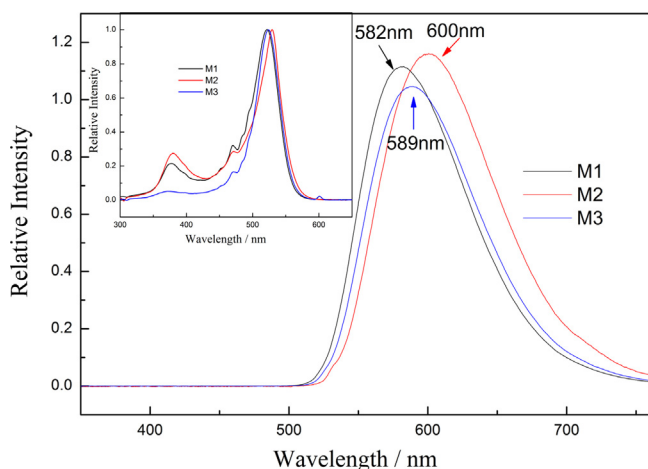


Fig. 4. The n-doping process and p-doping process of the three polymers at a scan rate of  $100 \text{ mV s}^{-1}$ .



**Fig. 5.** Fluorescence emission spectra of the **M1** (a), **M2** (b) and **M3** (c) dissolved in DMF. Inset: the fluorescence excitation spectra of the three monomers.

### 3.3. Fluorescence characteristics of monomers

Fluorescence test is another method to evaluate the characteristics of monomers. The fluorescence spectra of the monomers dissolved in DMF are illustrated in Fig. 5. The test results showed that all three monomers are good shiners. **M1**, **M2** and **M3** exhibited a strong excitation peak in visible region at 521 nm, 529 nm and 524 nm, respectively. While their emission peaks were observed at 582 nm, 600 nm and 589 nm, respectively. In all three

cases, the emission maxima experienced a bathochromic shift relative to their excitation maxima, indicating a Stokes shift values of 61 nm, 71 nm, and 65 nm for **M1**, **M2** and **M3** respectively. The relatively small red shift observed for the monomers suggests that there is little geometric change between the ground and excited states. It is interesting to find that the excitation and emission of all the monomers lie in the visible region, implying favorable photoluminescence properties of soluble monomers dissolved in DMF [21].

### 3.4. Morphology

Scanning electron micrographs (SEM) of polymers provide their clear surface and bulk morphologies, which are two important aspects closely related to their optical and electrical properties, such as charge transport and counterions storage capability. Fig. 6 gives the SEM images of **P1**, **P2** and **P3**, which were prepared potentiostatically in the solution of 0.2 M TBAPF<sub>6</sub> ACN/DCM containing relevant monomers on ITO electrodes with a charge of 0.1 C and dedoped before characterization. **P1** film exhibits a compact structure with lots of globules pervading on the surface and the approximate diameters of these globules are in the range of 2000–5000 nm. **P2** film shows a porous structure like coral grown with small granules, some holes are also found on the surface. While **P3** film exhibits a globular cluster structure with scattered holes between the clusters. The morphologies can facilitate the movement of doping anions into and out of the polymer film during doping and dedoping, which has a great influence on the optical and electrical properties of polymer films. In addition, the thicknesses of the three polymer films were measured by Step Profiler ((see Fig. S8 in Supporting Informations)). The thicknesses

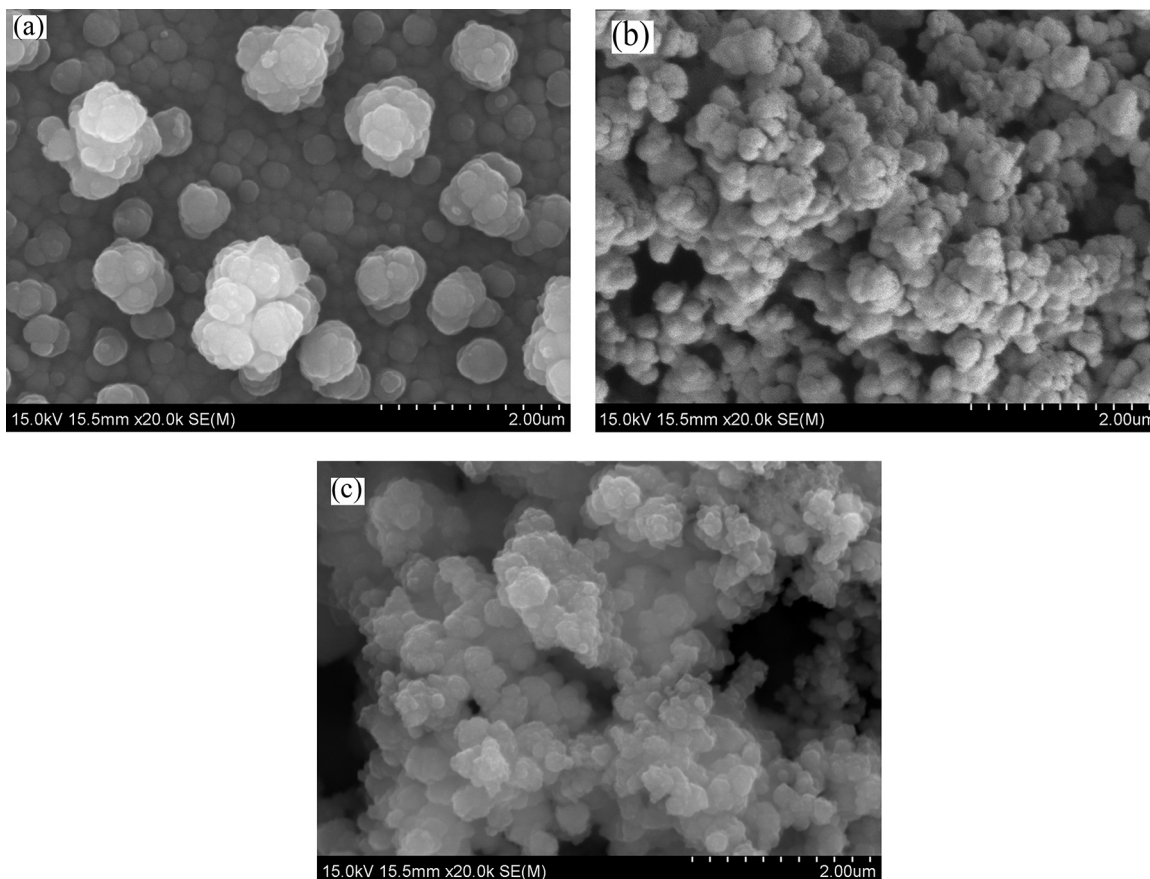


**Fig. 6.** SEM images of **P1** (a), **P2** (b) and **P3** (c) deposited potentiostatically onto ITO electrode.

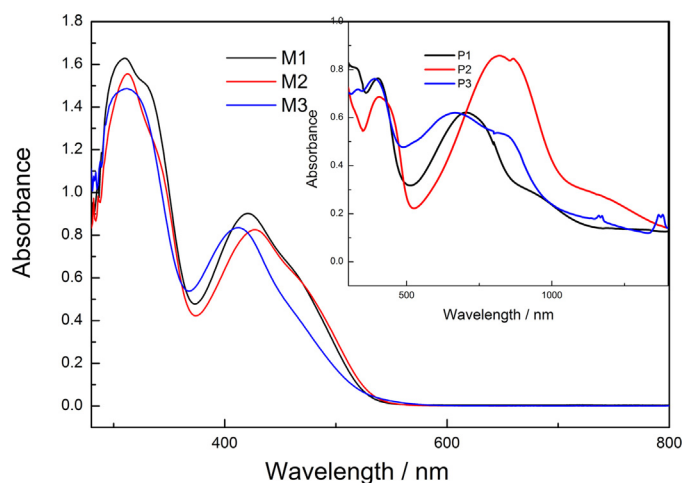


**Fig. 7.** UV–vis spectra of **M1**, **M2** and **M3** in DCM. Insert: absorption spectra of the corresponding polymers deposited on ITO at the neutral state.

are calculated as 823 nm, 708 nm and 678 nm for **P1**, **P2** and **P3**, respectively. The rugged scanning curves indicated the uneven surfaces of the films, which in good agreement with the morphologies given above.

### 3.5. Optical properties of the monomers and polymer films

**Fig. 7** illustrated the UV–vis spectra of **M1**, **M2** and **M3** monomers in DCM and their corresponding polymer films at the neutral state. The films were potentiostatically electrodeposited onto ITO glass with the same polymerization charge of  $2.5 \times 10^{-2} \text{C}$  in a mixed solution of DCM/ACN containing 0.005 M monomers and 0.2 M TBAPF<sub>6</sub> at 1.35 V, 1.1 V and 1.35 V, respectively. After polymerization, electrochemical dedoping of the films was respectively performed at 0 V, -0.4 V and 0 V in a solution of DCM/ACN containing only 0.2 M TBAPF<sub>6</sub> for a while, then washed with ACN/DCM for several times to remove the supporting electrolyte and oligomers/monomers.

The shape of the absorption spectra for either monomers or their corresponding polymers is quite similar to each other. Without any exception, all three monomers exhibited two distinct absorption bands, which could be accounted for the strong  $\pi$ - $\pi^*$  transition and intramolecular charge transfer band, respectively [22]. The two absorption peaks were appeared at 310 nm and 423 nm for **M1**, 313 nm and 427 nm for **M2**, 310 nm and 412 nm for **M3**. Their corresponding polymer films also displayed two absorption bands centered at 401 nm and 704 nm for **P1**, at 405 nm and 822 nm for **P2**, at 391 nm and 656 nm for **P3**. Compared the monomer with its corresponding polymers, a bathochromic shift was observed for all three cases, which may be

assigned to a result of J-aggregation [23]. There was a bit red shift observed when compared **M1** with **M2**, which can be attributed to the strong electron-donating group of 3-methoxythiophen. However, comparing **M3** to **M2**, a little small blue shift was observed, which caused by the steric hindrance effect as mentioned previously. Similarly, an obvious bathochromic shift of the maximum absorption wavelengths was observed in the case of **P2** when compared with both **P1** and **P3**.

**Table 1** summarized the electrochemical parameters of the three monomers and their corresponding polymer films, containing the onset oxidation potential ( $E_{\text{onset}}$ ), maximum absorption wavelength ( $\lambda_{\text{max}}$ ), low energy absorption edges ( $\lambda_{\text{onset}}$ ), HOMO and LUMO energy levels and optical band gap ( $E_{\text{g}}$ ) values. The HOMO energy level could be achieved by using the formula  $\text{HOMO} = -e(E_{\text{ox,onset}} + 0.02 + 4.4)$ . Herein, the number 0.02 in the formula is a correction parameter due to the reference electrode used in the experiments was not standard electrode. So before and after each experiment, the silver pseudo reference was calibrated versus the ferrocene redox couple and then adjusted to match the SCE reference potential. For DCM: ACN=1:1(v:v), the adjusted value is 0.02 while for DCM: ACN=1:9(v:v), the value is -0.098. Among the three monomers, **M2** possesses the lowest band gap while **M3** owns the highest band gap. For comparing, the band gaps of the three monomers were calculated by the density functional theory (DFT) level employing the Gaussian 09 programs. The ground-state electron density distribution of the highest occupied molecular orbital (HOMO) and lowest unoccupied molecular orbital (LUMO) are illustrated in **Fig. 8**. The HOMO and LUMO orbitals largely delocalized on the aromatic rings, forming a large conjugated system. The obtained band gap values were also listed

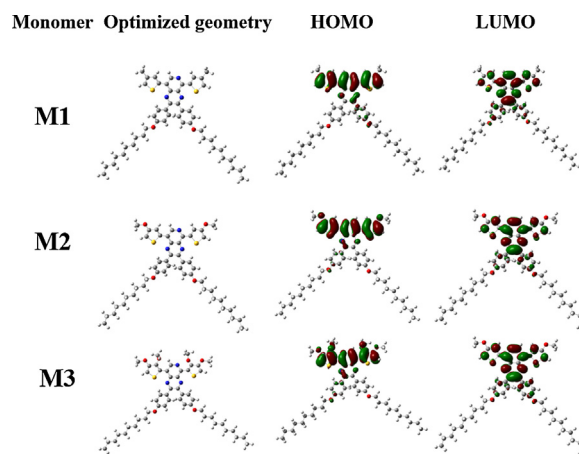


**Fig. 8.** The optimized geometries and the molecular orbital surfaces of the HOMOs and LUMOs for **M1**, **M2** and **M3**.

**Table 1**  
The onset oxidation potential ( $E_{\text{onset}}$ ), absorption onsets wavelength ( $\lambda_{\text{onset}}$ ), HOMO and LUMO energy levels and optical band gap ( $E_{\text{g}}$ ) of the monomers and their corresponding polymers.

Compounds	$E_{\text{onset,vs. (Ag wire)}}(\text{V})$	$\lambda_{\text{onset}}(\text{nm})$	$E_{\text{g,op}}^{(a)}(\text{eV})$	HOMO(eV)	LUMO <sup>(b)</sup> (eV)	$E_{\text{g,cal}}^{(c)}(\text{eV})$
M1	1.17	540	2.298	-5.59	-3.292	2.812
M2	0.91	541	2.294	-5.33	-3.036	2.773
M3	1.1	536	2.315	-5.52	-3.205	2.898
P1	0.425	890	1.39	-4.727	-3.37	–
P2	-0.03	1092	1.136	-4.39	-3.254	–
P3	0.76	990	1.25	-5.062	-3.812	–
P(A) <sup>(d)</sup>	–	–	1.4	–	–	–

<sup>(a)</sup>  $E_{\text{g,op}} = 1241/\lambda_{\text{onset}}$ , in which  $\lambda_{\text{onset}}$  refers to the low energy absorption edges.

<sup>(b)</sup> LUMO energy level was obtained by using the formula  $\text{LUMO} = -|\text{HOMO} - E_{\text{g}}|$ , where HOMO and  $E_{\text{g}}$  refer to the absolute value.

<sup>(c)</sup>  $E_{\text{g,cal}}$  was calculated by DFT calculations.

<sup>(d)</sup> See the reference [7].

in Table 1. The highest band gap is observed for **M3** and lowest is for **M2**, which is well consistent with the band gaps size order calculated from the lower energy absorptions. These values were found to be nearly 0.47 to 0.58 eV higher than the values from experimentally data. This is mainly due to various effects such as solvent effects and other experimental conditions. The band gap of **M3** is higher than that of both **M1** and **M2**, which hinted that steric hindrance of substituents on the thiophene ring of the oligomers may have decreased the population of the quinoidal electronic configuration and weakened intermolecular charge transfer, then affected the optical properties of the monomers.

From the Table 1, it can be seen that all three polymer films had relatively low band gaps which made them to be good candidates for electronic devices. The band gap of **P1** was somewhat higher than those of both **P2** and **P3**, which can be assigned to the poor electronic donating ability of the methyl group on the thiophene ring. **P2** had the lowest optical band gap (about 1.136 eV) among them. It is generally accepted that increasing the planarity and conjugation of aromatic systems leads to a decrease in the energy gap. Out of our expectation, **P3** had a higher band gap (about 1.25 eV) than **P2**. This can be attributed to that the introduction of four methoxy-group substituents on the thiophene ring causes steric hindrance, resulting in less order and less conjugation by the blue shift in the absorption spectra and the increase in polymer's band gap [22]. The results above suggest that as the donor unit, 3-methoxythiophen maybe have a more brilliant future than 3-methylthiophen and 3,4-dimethylthiophen do. Nevertheless, the band gap of anyone among the three polymers is lower than that of the previously reported polymer P(A) [7], whose band gap value

was 1.4 eV, indicating that all three polymers are promising candidates for organic photovoltaic applications.

### 3.6. Electrochromic properties of the polymers

UV-vis absorption spectra of three polymer films on ITO coated slide glass (the active area was  $0.9\text{ cm} \times 3.0\text{ cm}$ ) with the same polymerization charge of  $2.5 \times 10^{-2}\text{ C}$  were performed by holding the film at the desired potential and measuring the absorbance from 350 to 2200 nm with applied potentials ranging from -0.4 V to 1.2 V for **P2** and 0 V to 1.35 V for both **P1** and **P3** respectively for p-doping in a monomer-free 0.2 M TBAPF<sub>6</sub>/ACN/DCM solution.

Fig. 9 revealed spectroelectrochemistry and the corresponding colors of electrochemically prepared three polymer films at neutral and doped states. At neutral state, all of the three polymer films showed two absorption peaks, which was the nature of donor-acceptor systems. The high-energy peaks, which are attributed to the transitions from the thiophene-based valence band to its antibonding band, are mainly absorbing in the UV-region, with minor tailing into the visible region, limiting the contribution of the high-energy peak to the color perceived by the human eye. On the other hand, the low-energy peaks, originating from the D-A interaction, have pronounced absorption in the red part of the visible region, making the polymers appear blue in the reduced state. For **P2**, two well-separated absorption peaks were located at 408 nm and 820 nm, with a deep valley at 520 nm, which gives the polymer a green color as the green light is not absorbed and is allowed to pass through the film. Moreover,  $\pi$ - $\pi^*$  interaction between donor and acceptor determines the match between these units and plays a crucial role on the electronic properties of the

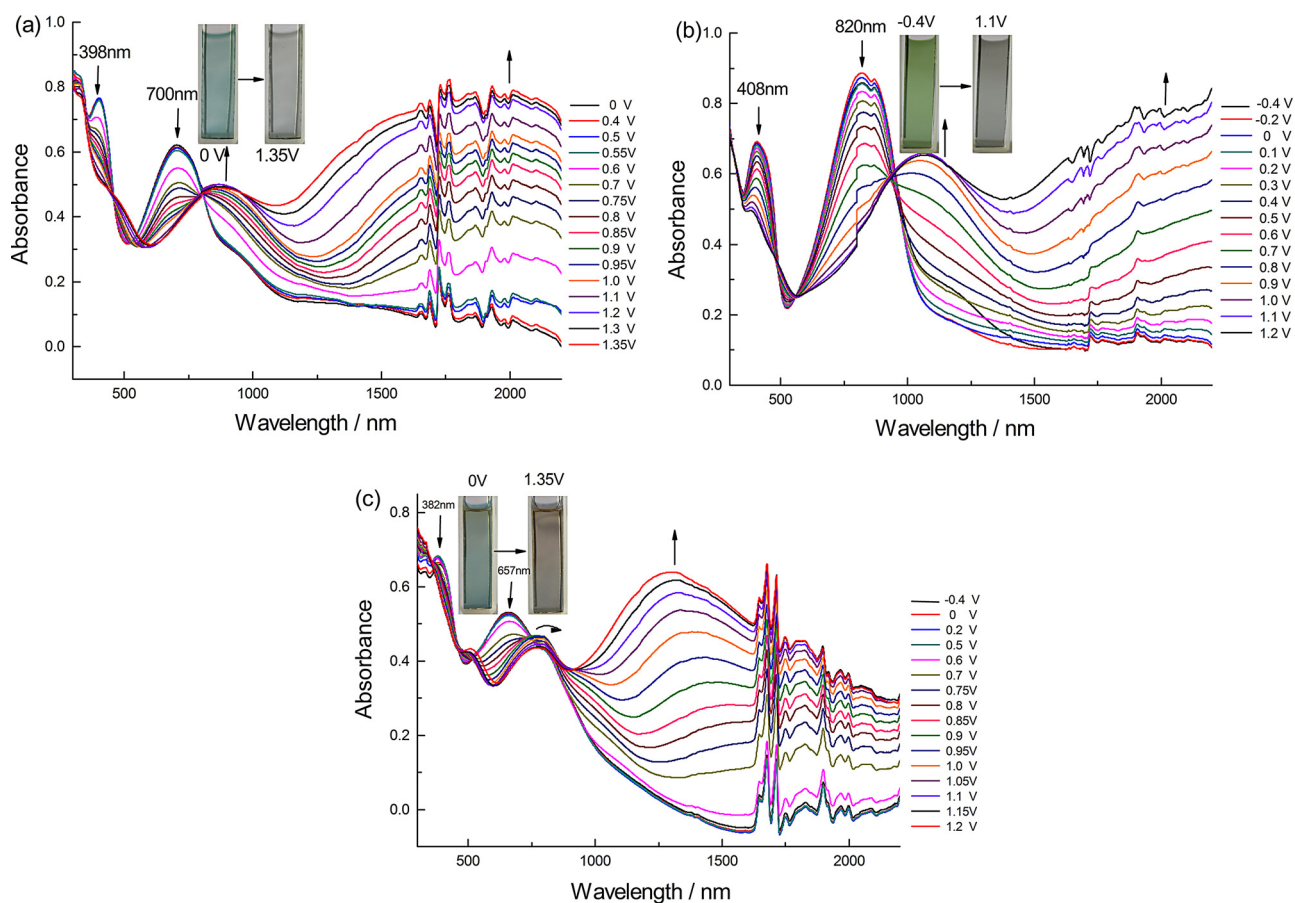


**Fig. 9.** The spectroelectrochemistry of films' p-doping processes on ITO electrode as applied potentials between 0 V and 1.35 V for **P1** (a), between -0.4 V and 1.1 V for **P2** (b) and between 0 V and 1.35 V for **P3** (c) in the monomer-free 0.2 M TBAPF<sub>6</sub>/ACN/DCM solution.

**Table 2**

The colorimetry analysis of the three polymer in both neutral and oxidized states.

Polymers	E,vs. (Ag wire)(V)	L	a	b	Color
P1	0	60	-12	1	Blue
	1.35	65	-2	2	Colorless
P2	-0.4	52	-16	27	Green
	1.1	58	-1	3	Light gray
P3	0	56	-7	2	Blue
	1.35	50	2	2	Light brown

resulting polymers since it influences the intramolecular charge transfer in these types of polymers. For **P1** and **P2**, the intensities for high-energy transitions and low-energy transitions are comparable with each other, indicating the ideal match between the donor and acceptor units and the strong interactions between them. Additionally, isosbestic points at around 804 nm for **P1** and 957 nm for **P2** confirmed the coexistence of more than one charged species absorbing in the visible region on the polymer chain.

Upon oxidation process of the three polymer films, the absorptions in the visible region started to decrease and new bands were intensified due to the formation of lower energy charge carriers such as polarons and bipolarons on the polymer backbone, along with a color change. In-situ spectroelectrochemical studies for the polymer films showed that during oxidation the color of the film changed from a transmissive light blue to colorless for **P1**, from green to a transparent light gray color for **P2** and from blue to a transmissive brown color for **P3**. Color is made up of three

attributes: hue (a), saturation (b) and luminance (L). The values of the relative luminance (L) and a, b were measured at the neutral and oxidized states of the three polymers and summarized in **Table 2**. The color is less transmissive for **P2** than that of **P1** in oxidized state, which due to the polaronic absorption band of **P1** tailed more into the visible region. It is worth mentioning that **P2** film is unique in the literature with its highly saturated green color in the neutral state and exceptional transparency in the oxidized state. In addition, compared with **P2**, both the electron poor homologue **P1** and the electron strong homologue **P3** revealed blue shifted dominant wavelengths in visible and in NIR regions which were consistent with electrochemical data.

Based on the discussion above, a conclusion can be drawn that the different structures of the polymers due to the difference in donor moiety affect not only the monomer oxidation and the polymer redox couple potentials but also the maximum absorption wavelengths of the corresponding transition.

### 3.7. Electrochromic switching studies

Optical contrast (or percent transmittance, refers to the percentage transmittance change ( $\Delta T\%$ ) at a specified wavelength), switching time (or response time, defined as the necessary time for 95% of the full optical switch), stability (or cycle life) and coloration efficiency are very important parameters to evaluate electrochromic materials. They were analyzed by changes that occurred in the transmittance (increments and decrements of the absorption band at a specified wavelength with respect to time)

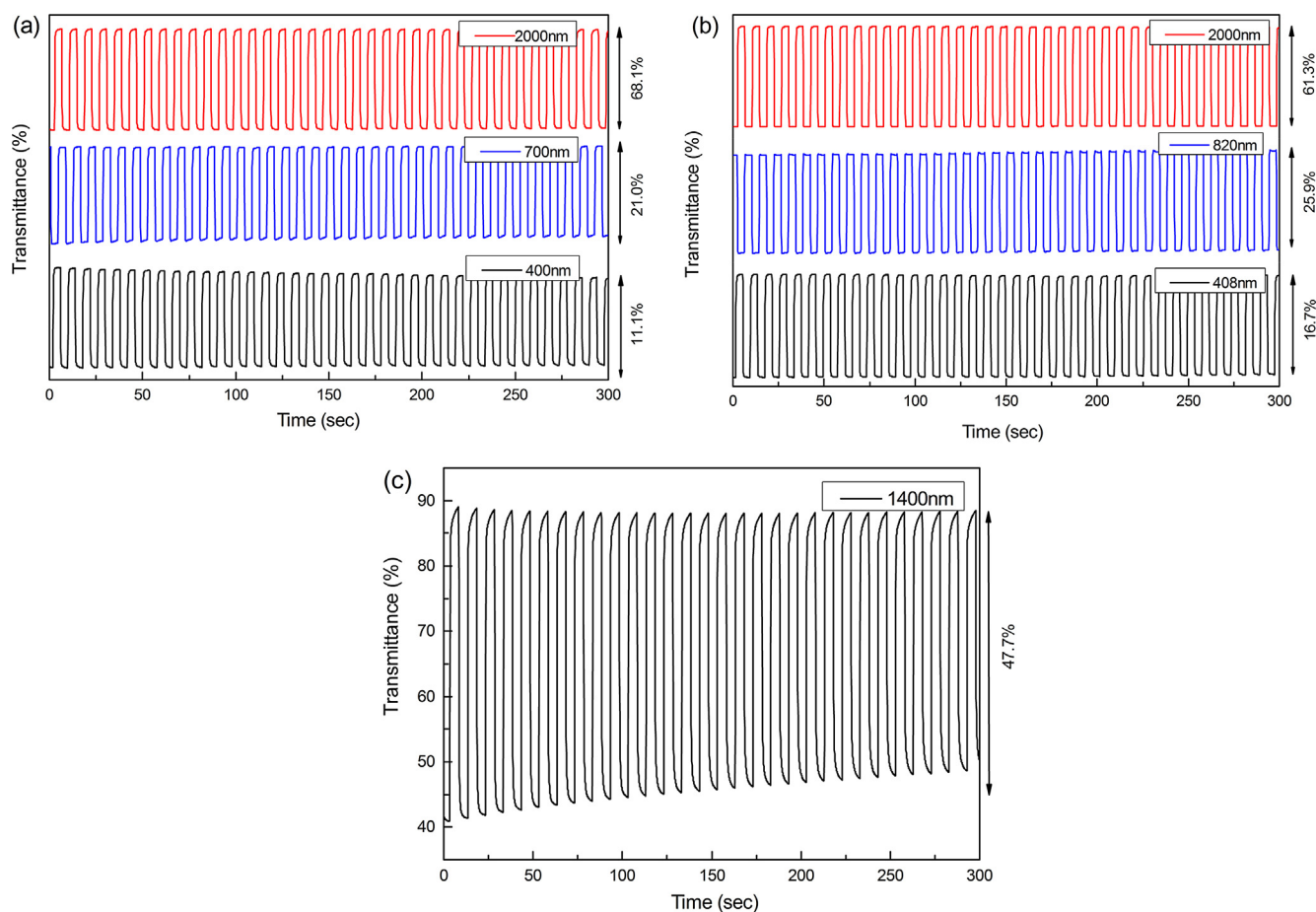


**Fig. 10.** (a) Electrochromic switching, percent transmittance change monitored at 400, 700 and 2000 nm for **P1** between 0 V and 1.35 V. (b) Electrochromic switching, percent transmittance change monitored at 408, 820 and 2000 nm for **P2** between -0.4 V and 1.1 V. (c) Electrochromic switching, percent transmittance change monitored at 1400 nm for **P3** between 0 V and 1.35 V.

**Table 3**

The optical contrasts and response times from neutral state to oxidation state of the three polymers.

Polymer	$\lambda$ /nm	Optical contrast/%	Response time/s
P1	400	11.1	0.88
	700	20.1	0.88
	2000	68.1	0.46
P2	408	16.7	0.61
	820	25.9	0.55
	2000	61.3	0.35
	P3	1400	47.7
P(A)	1490	50	–
	2000	18	–

while switching the potential step wisely between the neutral state and oxidized state with a residence time of 4 s.

Fig. 10 exhibited the optical contrast of the three polymer films at different wavelengths. The polymer film was potentiostatically deposited onto ITO-coated glass (active area: 0.9 cm × 3.0 cm) with the polymerization charge of  $1.5 \times 10^{-2}$  C in the same manner as described above. After regular switching for 300 s, there was no distinct loss in percent transmittance contrast observed, which manifested the high stabilities of all three polymer films. The optical contrast and the response times from reduced to oxidized state of the three polymer films at different wavelengths were summarized in Table 3. As is shown in Table 3, all three polymer films revealed a relatively high optical contrast in NIR region which hinted a very significant character for various NIR applications. Comparing with P(A), our polymers have higher transmittance values, which indicated the promising potential applications in smart windows of polymers studied in this paper. P1 and P2 had such fast switching time that less than 1 s both in the visible and NIR region but the response time of P3 was more longer (over 2 s) than that of P1 and P2. This is a further indication that the electrochromism property of P3 is not as good as that of P1 and P2.

Coloration efficiency (CE) is another key parameter to evaluate the properties of polymer films as it describes the change in optical absorbance at the wavelength of interest to the density of injected/ejected charge [24]. It is defined as the change in the optical density ( $\Delta OD$ ) for the charge consumed per unit electrode area ( $\Delta Q$ ) [25]. The calculating equations were given below:

$$\Delta OD = \log\left(\frac{T_b}{T_c}\right) \text{ and } \eta = \frac{\Delta OD}{\Delta Q}$$

Where  $T_b$  and  $T_c$  are the transmittances before and after coloration, respectively, and  $\eta$  denotes the coloration efficiency (CE). The coloration efficiency was measured as  $94.8 \text{ cm}^2 \text{ C}^{-1}$  at 400 nm,  $100.0 \text{ cm}^2 \text{ C}^{-1}$  at 700 nm and  $269.7 \text{ cm}^2 \text{ C}^{-1}$  at 2000 nm for P1. And for P2, CE was calculated as  $87 \text{ cm}^2 \text{ C}^{-1}$  at 408 nm,  $161.8 \text{ cm}^2 \text{ C}^{-1}$  at 820 nm,  $309.6 \text{ cm}^2 \text{ C}^{-1}$  at 2000 nm. For P3, CE was counted as  $507.7 \text{ cm}^2 \text{ C}^{-1}$  at 1400 nm. All the results calculated above were reasonable coloration efficiency.

For electrochromic applications, the ability of a polymer to switch rapidly and to exhibit a striking color change and maintain high stability upon repeated cycles is important. Considering the above discussion, a summing-up can be made that all three polymer films have high optical contrast, fast switching time and satisfactory coloration efficiency, which make them to be better candidates in electrochromic display applications, especially in the field of smart windows.

#### 4. Conclusion

In this study, three new type electrochromic polymers containing pyrido[4,3-b]pyrazine group (acceptor) and different

thiophen derivatives (donor) were synthesized to understand the effects of different electron donating groups on electrochemical and optoelectronic properties. The results suggested that the influence of donor units for D-A type polymer properties were related to many factors such as electron-donating ability, steric hindrance and the match between donor and acceptor units. At neutral state, P1, P2 and P3 showed a transmissive light blue, green and blue color, respectively. And all the three polymers are almost colorless and highly transmissive in their oxidized states with a strong absorption in the IR region. This property may ease several applications for NIR electrochromic devices. Furthermore, P2 had the lowest band gap (about 1.136 eV) among the three polymers, which demonstrated the excellent match between the acceptor unit and the donor one. In addition, all three polymers revealed high optical contrast, fast switching time and satisfactory coloration efficiency, especially in the case of P2. Taking all above into account, the three polymers are outstanding candidates for the potential realization of RGB-based polymer electrochromic device applications.

#### Acknowledgements

The work was financially supported by the National Natural Science Foundation of China (51473074, 31400044), the General and Special Program of the postdoctoral science foundation China (2013M530397, 2014T70861)

#### Appendix A. Supplementary data

Supplementary data associated with this article can be found, in the online version, at <http://dx.doi.org/10.1016/j.electacta.2014.09.022>.

#### References

- [1] R.J. Mortimer, A.L. Dyer, J.R. Reynolds, Displays 27 (2006) 2–18, doi:<http://dx.doi.org/10.1016/j.displa.2005.03.003>.
- [2] A. Azens, C.G. Granqvist, J. Solid State Electrochem. 7 (2003) 64–68, doi:<http://dx.doi.org/10.1007/s10008-002-0313-4>.
- [3] N. Stutzmann, R.H. Friend, H. Sirringhaus, Science 299 (2003) 1881–1884, doi:<http://dx.doi.org/10.1126/science.1081279>.
- [4] D.T. McQuade, A.E. Pullen, T.M. Swager, Chem. Rev. 100 (2000) 2537–2574, doi:<http://dx.doi.org/10.1021/cr9801014>.
- [5] S. Möller, C. Perlov, W. Jackson, C. Taussig, S.R. Forrest, Nature 426 (2003) 166–169, doi:<http://dx.doi.org/10.1038/nature02070>.
- [6] W. Walker, B. Veldman, R. Chiechi, S. Patil, M. Bendikov, F. Wudl, Macromolecules 41 (2008) 7278–7280, doi:<http://dx.doi.org/10.1021/ma8004873>.
- [7] M. Nikolou, A.L. Dyer, T.T. Steckler, E.P. Donoghue, Z.C. Wu, N.C. Heston, A.G. Rinzler, D.B. Tanner, J.R. Reynolds, Chem. Mater. 21 (2009) 5539–5547, doi:<http://dx.doi.org/10.1021/cm902768q>.
- [8] A. Balan, D. Baran, G. Gunbas, A. Durmus, F. Ozyurt, L. Toppare, Chem. Commun. (2009) 6768–6770, doi:<http://dx.doi.org/10.1039/B912482A>.
- [9] A.P. Zoombelt, M.A.M. Leenen, M. Fonrodona, Y. Nicolas, M.M. Wienk, R.A.J. Janssen, Polymer 50 (2009) 4564–4570, doi:<http://dx.doi.org/10.1016/j.polymer.2009.07.028>.
- [10] P. Sakhthivel, H.S. Song, N. Chakravarthi, J.W. Lee, Y.S. Gal, S. Hwang, Polymer 54 (2013) 4883–4893, doi:<http://dx.doi.org/10.1039/C4TA2585G>.
- [11] S. Toksabay, S.O. Hacioglu, N.A. Unlu, A. Cirpan, L. Toppare, Polymer, 55 309 (2014) 3093–3099, doi:<http://dx.doi.org/10.1016/j.polymer.2014.05.029>.
- [12] A.T. Taskin, A. Balan, B. Epik, E. Yildiz, Y.A. Udum, L. Toppare, Electrochim. Acta 54 (2009) 5449–5453, doi:<http://dx.doi.org/10.1016/j.electacta.2009.04.042>.
- [13] Y. Lee, Y.M. Nam, W.H. Jo, J. Mater. Chem. 21 (2011) 8583–8590, doi:<http://dx.doi.org/10.1039/C1JM10877H>.
- [14] C.J. DuBois, K.A. Abboud, J.R. Reynolds, J. Phys. Chem. B 108 (2004) 8550–8557, doi:<http://dx.doi.org/10.1021/jp037013u>.
- [15] G. Sonmez, I. Schwendeman, P. Schottland, K. Zong, J.R. Reynolds, Macromolecules 36 (2003) 639, doi:<http://dx.doi.org/10.1021/ma021108x>.
- [16] G.E. Gunbas, A. Durmus, L. Toppare, Adv. Funct. Mater. 18 (2008) 2026–2030, doi:<http://dx.doi.org/10.1002/adfm.200701386>.
- [17] Z. Xu, M. Wang, J.S. Zhao, C.S. Cui, W.Y. Fan, J.F. Liu, Electrochim. Acta 125 (2014) 241–249, doi:<http://dx.doi.org/10.1016/j.electacta>.
- [18] B.-L. Lee, T. Yamamoto, Macromolecules 32 (1999) 1375, doi:<http://dx.doi.org/10.1021/ma981013o>.

- [19] M. Ak, M.S. Ak, G. Kurtay, M. Güllü, L. Toppare, *Solid State Sci.* 12 (2010) 1199–1204, doi:<http://dx.doi.org/10.1016/j.solidstatesciences.2010.03.013>.
- [20] C.J. DuBois, J.R. Reynolds, *Adv. Mater.* 14 (2002) 1844, doi:<http://dx.doi.org/10.1002/adma.200290016>.
- [21] L.Y. Xu, J.S. Zhao, R.M. Liu, H.T. Liu, J.F. Liu, H.S. Wang, *Electrochim. Acta* 55 (2010) 8855–8862, doi:<http://dx.doi.org/10.1016/j.electacta.2010.08.044>.
- [22] C.M. Amb, A.L. Dyer, J.R. Reynolds, *Chem. Mater.* 23 (2011) 397–415, doi:<http://dx.doi.org/10.1021/cm1021245>.
- [23] H. Yamagata, F.C. Spano, *J. Chem. Phys.* 136 (2012) 184–901, doi:<http://dx.doi.org/10.1063/1.4705272>.
- [24] P.M. Beaujuge, J.R. Reynolds, *Chem. Rev.* 110 (2010) 268–320, doi:<http://dx.doi.org/10.1021/cr900129a>.
- [25] M. Deepa, A. Awadhia, S. Bhandari, *Phys. Chem. Chem. Phys.* 11 (2009) 5674–5685, doi:<http://dx.doi.org/10.1039/B900091G>.